Research in Astronomy and Astrophysics, 24:015019 (8pp), 2024 January https://doi.org/10.1088/1674-4527/ad0b84

Simulation of RFI Cancellation Using Subspace Projection Algorithm for PAF Receiver

Peng Wu[1,2,3], Jian Li[1,3], and Mao-Zheng Chen[1,3,4]
[1] Xinjiang Astronomical Observatory, Chinese Academy of Sciences, Urumqi 830011, China; wupeng@xao.ac.cn, chen@xao.ac.cn
[2] University of Chinese Academy of Sciences, Beijing 100049, China
[3] Xinjiang Key Laboratory of Microwave Technology, Urumqi 830011, China
Received 2023 June 5; revised 2023 September 18; accepted 2023 October 13; published 2024 January 9

Abstract

The simulation of radio frequency interference (RFI) cancellation by applying a spatial filtering technique for phased array feed (PAF) is presented. In order to better reflect the characteristics of PAF, a new signal model is to add the coupling coefficient among elements of PAF to the conventional array signal model. Then the subspace projection (SP) algorithm is used to cancel RFI from the correlation matrix of the signal, and finally, the 2D power image is drawn. The power variation of signal-of-interest direction and RFI direction before and after using the SP algorithm is analyzed. The new signal model and simulation strategy can be used to test and verify the beamformer.

Key words: methods: analytical – techniques: radar astronomy – telescopes

1. Introduction

A phased array feed (PAF) receiver, as an example of the next generation microwave receiving system, has been widely studied all over the world. However, the applications of spatial interference cancellation using PAF are rare in radio astronomy (Wang et al. 2021). At present, most radio frequency interference (RFI) mitigation methods are for narrow-band and pulsed or intermittent interfering signals, these are based on a time-frequency character of the signal and the RFI are normally blanked. In this paper, the simulation of RFI mitigation based on spatial information using the PAF receiver is presented. A signal model with planar coupling effect is established, and the effect on the main beam is analyzed. The subspace projection (SP) algorithm is used to simulate PAF receiver cancellation RFI and the performance of output power is studied in signal-of-interest (SOI) and RFI directions.

The SP algorithm is used to simulate PAF mitigation RFI and performance of output power in different directions is studied. Different from conventional array, PAF is a tightly distributed array designed for reflector antennas. The conventional array signal model cannot include a coupling effect among elements of PAF. This paper presents the performance of the PAF coupling effect in data correlation operation from baseband data. Then, radio telescope pattern and RFI cancellation are simulated and analyzed by combining antenna simulation software, the MaxSNR and SP algorithms.

The Mk II PAF receiver developed for ASKA by the Commonwealth Science and Industrial Research Organization in Australia has been compressed from 0.8–1.74 GHz to 1.2–1.75 GHz due to interference from mobile phone and digital television signals after Parkes and Effelsberg tests (Chippendale et al. 2016). The American FLAG project considered adaptive filtering technology to mitigate RFI in beamforming and verified the performance of Linear Constraint Minimal Variance (LCMV) and SP algorithms in PAF (Warnick et al. 2007; Landon et al. 2012). Now, there is no PAF receiver fully put into use in China, but several research projects and groups, including the Five-hundred-meter Aperture Spherical radio Telescope (FAST) team of the National Astronomical Observatories (Chai et al. 2020) and Qi Tai Telescope (QTT) project (Wang 2014), are rapidly carrying out research.

QTT, the largest fully steerable single dish radio telescope currently under construction in the world, has been selected by *Nature* as the most noteworthy science project in 2023.[5] Its prime focus will be equipped with a 96-element dual-polarization PAF array. (Ma et al. 2019), where beamforming will be implemented in GPU of digital terminal (Pei et al. 2022). There is no doubt that this PAF receiver is the most complex system in QTT, and its development is full of challenges. However, a suitable numerical model can be used for theoretical analysis, validation, or improvement of beamforming algorithms, etc. Therefore, a baseband numerical model and algorithm simulation that can reflect the characteristics of the PAF receiver become meaningful. Ivashina et al. (2011) optimized the joint field of view and beam rotational symmetry of PAF receiver through numerical simulations in the Westerbork Synthesis Radio Telescope (WSRT) project.

[4] Author to whom any correspondence should be addressed.

[5] https://www.nature.com/articles/d41586-022-04444-3

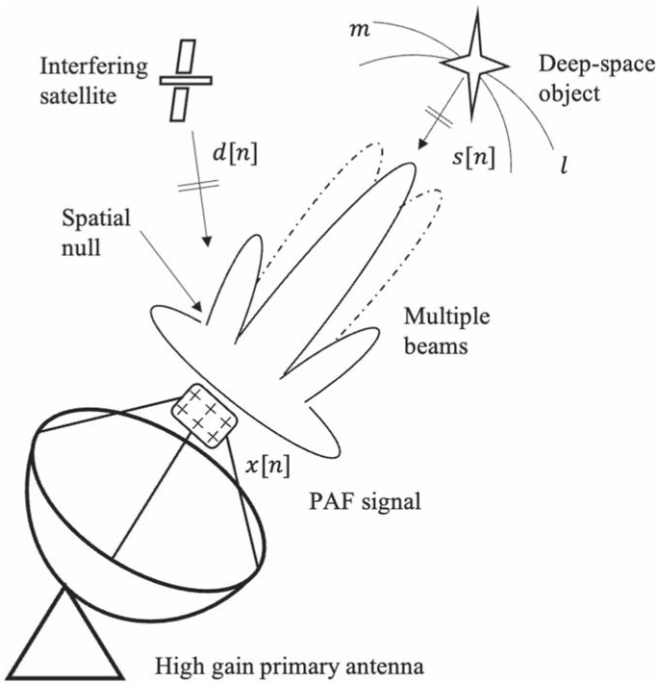

Figure 1. The main advantages of PAF are that multiple beams can be formed simultaneously to provide joint field of view, actively control the number and shape of the beams, and spatial cancellation of interference.

Landon et al. (2012) studied the improvement of the SP algorithm for moving RFI in numerical simulation. The coupling effect of PAF was not considered in these signal models. Nybo Jeffrey (2019) established a signal model containing coupling characteristic in the FLAG project for the test and verification of GPU beamforming, but the signal model is a simple linear model, which is not suitable for planar array.

With the use and development of radio in people's production and life, there is an urgent need to deal with the ubiquitous interference, such as television signals, FM radio transmission, air navigation equipment. Even radio-quiet zones are not immune to man-made radio interference, such as satellite downlinks. As shown in Figures 1 and 2, PAF in radio astronomy provides a promising method. The spatial features of RFI can be extracted by sampling the focal plane field to track and remove interference without discarding data. Even interference sources that completely cover the astronomical signal spectrum can be canceled. This technique is expected to improve the capability of radio telescopes in the presence of interference.

The remainder of this paper is organized as follows. Section 2 provides the new model of PAF, detailed definition, and mathematical preparation of the SP beamforming. In Section 3 we customize a simulation strategy and verify the performance of new signal model in the main beam on the QTT-PAF model. The SP algorithm is used to cancel the data containing RFI in the beamformer, and power variation before and after using the SP algorithm is analyzed. Section 4 is a summary.

2. Preliminaries

2.1. Signal Model of PAF in Time

As depicted in Figure 2, assuming narrowband operation of an M element PAF, the $M \times 1$ complex baseband data vector at time n sample is given as

$$\boldsymbol{x}[n] = \boldsymbol{c}(\boldsymbol{a}s[n] + \boldsymbol{v}d[n] + \boldsymbol{n}[n]) \tag{1}$$

where $s[n]$ is the SOI with array response vector $\boldsymbol{a}$ (normalized spatial characteristics of celestial bodies in PAF, sometimes called array manifolds, including effects of the reflector dish and the geometry of PAF), $d[n]$ is the single interfering source with corresponding array response $\boldsymbol{v}$ (usually not in the direction of main focus). In general, $\boldsymbol{a}$ is constant because telescopes are mechanically controlled at the same line of sight as SOI. As the interferer is random or the dish tracks SOI, $\boldsymbol{v}$ is changing with time. $\boldsymbol{c}$ is the $M \times M$ matrix, which describes the coupling characteristic of PAF, and the following section will introduce in detail. Noise vector $\boldsymbol{n}[n]$ is assumed to be spatially non-white, Gaussian, and the correlation arises mainly from the PAF coupling effect. Signals $s[n]$, $d[n]$, and $\boldsymbol{n}[n]$ are assumed to be temporally wide sense stationary. Beamformer output $\boldsymbol{y}$ is the weight $\boldsymbol{w} = [w_1, w_2, ..., w_M]^H$ sum of signals received by each array element and is computed as

$$\boldsymbol{y} = \boldsymbol{w}^H \boldsymbol{x}. \tag{2}$$

2.2. Signal Correlation Analysis

Usually, the signal sampling rate is much faster than the movement of interference, so $\boldsymbol{v}$ is approximated to a constant in a short-time integration (STI). The SOI and RFI are supposed to be uncorrelated from each other. These should also be independent of the noise of each receiving chain. The covariance matrix of the signal in the jth STI window of length T samples is estimated to be

$$\begin{aligned}\hat{\boldsymbol{R}}_x &= \frac{1}{T}\sum_{n=jT}^{(j+1)T-1} \boldsymbol{x}[n]\boldsymbol{x}^H[n] = \frac{1}{T}\boldsymbol{X}_j\boldsymbol{X}_j^H \\ &= \underbrace{\boldsymbol{c}}_{Couple}(\underbrace{\boldsymbol{a}\boldsymbol{R}_s\boldsymbol{a}^H}_{R_{SOI}} + \underbrace{\boldsymbol{v}\boldsymbol{R}_r\boldsymbol{v}^H}_{R_{RFI}} + \underbrace{\boldsymbol{N}}_{R_{Noise}})\underbrace{\boldsymbol{c}^H}_{Couple}\end{aligned} \tag{3}$$

where:

1. $\boldsymbol{X}_j = [\boldsymbol{x}[jT], \boldsymbol{x}[jT+1], \cdots, \boldsymbol{x}[(j+1)T-1]]$ is the $M \times T$ matrix, the voltage output of PAF through the T sample points observation.
2. $\boldsymbol{N}$ is the $M \times M$ noise covariance matrix, supposed to be diagonal. We assume $N = \lambda^2\boldsymbol{I}$, where λ^2 is noise power and $\boldsymbol{I}$ is the identity matrix.

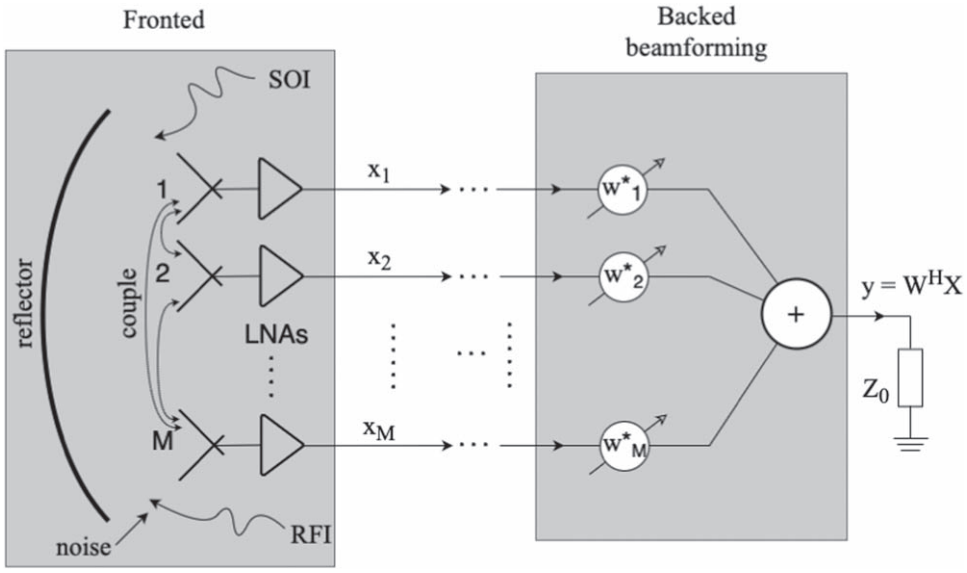

Figure 2. Generalized representation of PAF receiver.

3. $\boldsymbol{R}_s$ is the 1×1 SOI covariance matrix, which is also the power of SOI in an STI window. The generated SOI has Gaussian, centered, white and stationary characteristics.
4. $\boldsymbol{R}_r$ is the $Q \times Q$ RFI covariance matrix. Q is the number of interferer.
5. $\boldsymbol{c}$ is the $M \times M$ matrix, which is the coupling coefficient among the elements. The tight arrangement among elements of PAF increases the radiation bandwidth and destroys the beam pattern. The coupling phenomenon means that when a wave arrives at PAF, the induced current in one element will radiate some energy back to other elements in PAF. There is more induction among the near elements and less induction among the far elements. In the model in Figure 3, the elements are placed in the rectangular coordinate system, and the distance between two elements can be expressed by a tuple (Δx, Δy). At this time, when the signal of PAF is correlated, the coupling effect caused by the distribution of the elements can be assumed to be a covariance matrix $\mathfrak{C}$, which is expressed as follows:

$$\mathfrak{C} = \begin{bmatrix} \sigma\sqrt{\Delta x_{0,0}^2+\Delta y_{0,0}^2} & \sigma\sqrt{\Delta x_{0,1}^2+\Delta y_{0,1}^2} & \cdots & \sigma\sqrt{\Delta x_{0,M}^2+\Delta y_{0,M}^2} \\ \sigma\sqrt{\Delta x_{1,0}^2+\Delta y_{1,0}^2} & \sigma\sqrt{\Delta x_{1,1}^2+\Delta y_{1,1}^2} & \cdots & \sigma\sqrt{\Delta x_{1,M}^2+\Delta y_{1,M}^2} \\ \vdots & \vdots & \ddots & \vdots \\ \sigma\sqrt{\Delta x_{M,0}^2+\Delta y_{M,0}^2} & \sigma\sqrt{\Delta x_{M,1}^2+\Delta y_{M,1}^2} & \cdots & \sigma\sqrt{\Delta x_{M,M}^2+\Delta y_{M,M}^2} \end{bmatrix} \quad (4)$$

where σ is the coefficient of the coupling effect (generally determined by the inherent characteristics of the elements material). So $\boldsymbol{c}$ is the Cholesky decomposition matrix of $\mathfrak{C}$.

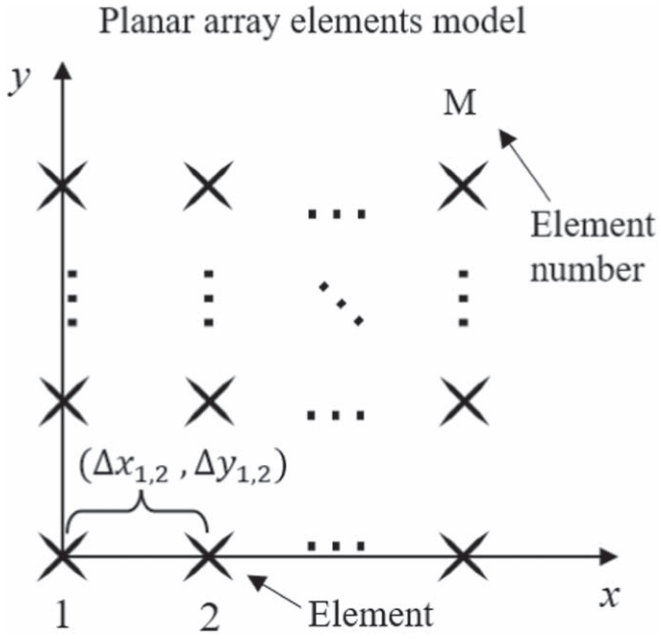

Figure 3. The layout of PAF elements in the plane.

2.3. The SP Algorithm

The mathematical principle of SP projection in the PAF receiver can be summarized as a linear transformation from one vector space to another.

Compared with the waveguide feed, the PAF receiver can extract the spatial characteristic (the position information) of a target signal, and the signal can be selectively mitigated or

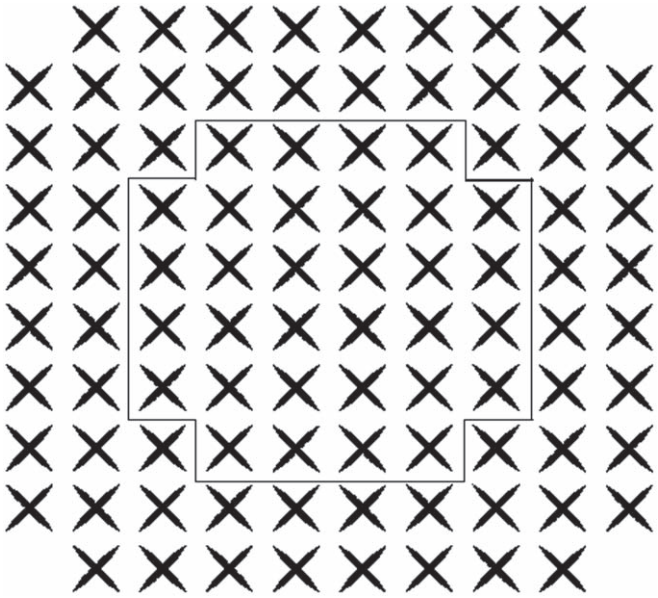

Figure 4. PAF model equipped with the QTT project consists of 96×2 elements. The selected elements in the figure are used for one beam.

accepted, which provides a new idea to cancel RFI for the single-aperture radio telescope. In this section, we will explain the working principle of the SP algorithm from the perspective of vector space of data. In an STI window, the expected value of the signal is estimated by the covariance matrix, and the spatial feature vector of RFI is extracted by the array information processing method. S is used to represent the output signal space of PAF. According to different radio astronomical signal processing targets, S can be divided into three subspaces, namely SOI subspace, RFI subspace, and noise subspace. The three subspaces are expressed as follows:

$$\begin{aligned} \Re(\boldsymbol{a}) &= O, \\ \Re([\boldsymbol{v}_1, \ldots, \boldsymbol{v}_Q]) &= V, \\ \Re(\boldsymbol{n}) = N = \Re(\boldsymbol{x}[n]) &= S. \end{aligned} \tag{5}$$

where $\Re(\cdot)$ represents the column space. We want to project the output signal of PAF into a special space W, which satisfies that W is perpendicular to V and W belongs to S. The matrix orthogonal projection method can be used, the expression is as follows:

$$\boldsymbol{P}^{\perp} = \boldsymbol{I} - \boldsymbol{v}(\boldsymbol{v}^H \boldsymbol{v})^{-1} \boldsymbol{v}^H \tag{6}$$

which is such that $\boldsymbol{P}^{\perp}\boldsymbol{v} = 0$. Therefore, when the spatial filter is applied to the data covariance matrix, all the energy due to interference will be nulled. The column space of $\boldsymbol{P}^{\perp}$ can be described as

$$\Re(\boldsymbol{P}^{\perp}) = W = \Omega - V \tag{7}$$

where the column space of $\boldsymbol{I}$ is the whole space $\Omega = \mathbb{R}^L$. It can be understood as finding a set of vector basis that does not contain RFI spatial feature, so that the projection value of some data containing RFI spatial feature on this set of vector basis is zeros.

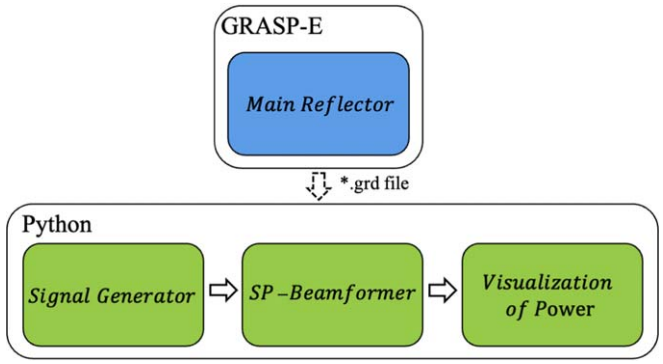

Figure 5. Flow chart of simulation strategy. GRASP-E simulation results are read by Python in the data format of *.grd.

Then, the $\boldsymbol{P}^{\perp}$ transform is performed on PAF weight $\boldsymbol{w}$ to obtain the weight vector $\boldsymbol{\omega}_{\perp}$ with RFI mitigation capability. The expression is as follows:

$$\boldsymbol{P}^{\perp}\boldsymbol{\omega} = \boldsymbol{\omega}_{\perp}. \tag{8}$$

In the linear transformation of Equation (8), $\boldsymbol{P}^{\perp}$ vertical has an important feature: idempotency, which determines that the projection only plays a role in the first mapping and does not superimpose multiple mapping effects.

3. Simulation

In this section, the simulation design is based on the PAF model in QTT. As shown in Figure 4, a detailed numerical model is used for 32 of the 96 elements. This scheme refers to the design of Ma et al. (2021). In this numerical model, we generate the data model described in Equation (1) and use that to realize the beamforming simulation and performance analysis of the SP algorithm canceling RFI.

3.1. Simulation Conditions

The tools we use in this simulation are the GRASP-E and Python. The former is a free version of a general purpose reflector antenna designed for students by TICRA company in Denmark,[6] and the latter is an open source data processing and drawing script language. The whole simulation strategy can be divided into four parts, and the flow chart of the simulation strategy is shown in Figure 5.

Main Reflector: GRASP-E is used to simulate the pattern of 110 m reflector. As the specific design details are not disclosed, the influence of the support structure is not considered in this simulation. Figures 6 and 7 list the reflector model and pattern.

[6] https://www.ticra.com/software/grasp-student-edition/

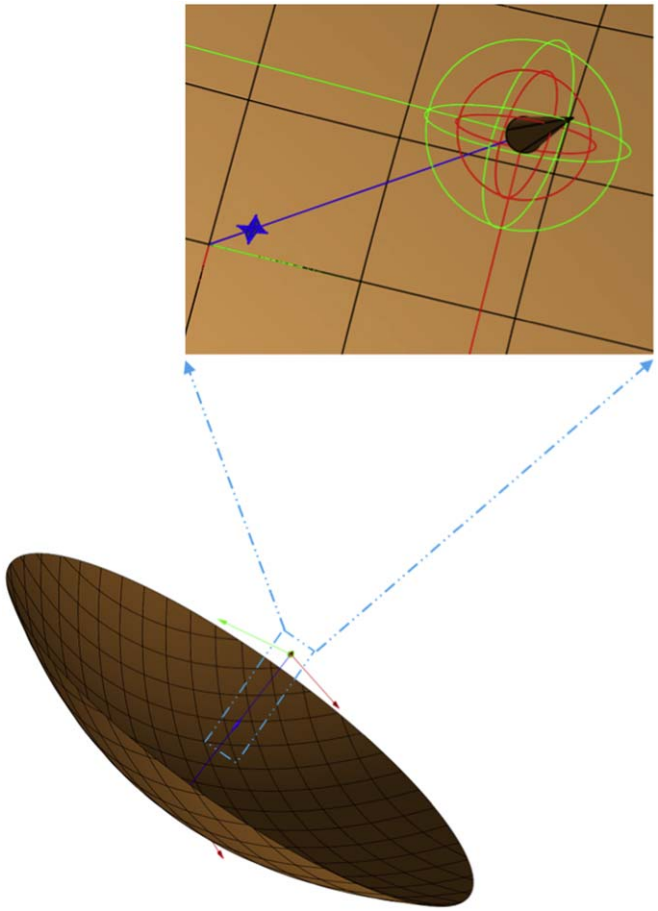

Figure 6. QTT 110 m paraboloid model, focal diameter ratio $f/d = 0.33$. The feed is conical and taper angle is 74°.29.

Signal Generator: The complex exponential signal of PAF including SOI, RFI, and noise is generated (Li et al. 2023), which satisfies the description in Equation (3) statistically. The main parameters of the *Signal Generator* in this simulation process are (a) the element's position parameter table (which largely determines the shape of the beam); (b) the proportional coefficient between the element's spacing and operating frequency; (c) the ratio of sampling rate to signal frequency; (d) the location information of SOI and RFI in space; (e) the SNR of SOI and RFI, where $\mathrm{SNR} = 10\log_{10}\frac{P_s}{P_n}$, P_s is signal power and P_n is noise power.

SP-Beamformer: The main purpose of this part is to calculate the vector $\boldsymbol{P}^{\perp}$ and to realize beamforming. $\boldsymbol{P}^{\perp}$ is the weight of MaxSNR $\boldsymbol{\omega}_{\mathrm{maxSNR}}$ reweighted, the expression is $\boldsymbol{\omega}_{\perp} = \boldsymbol{P}^{\perp}\boldsymbol{\omega}_{\mathrm{maxSNR}}$. It mainly includes signal covariance calculation, matrix decomposition, and other operations. The important parameters considered in this simulation process are (a) the size of STI window; (b) the normalized spatial characteristic of RFI. The error of measured estimated $\hat{\boldsymbol{v}}$ and $\boldsymbol{v}$ plays a key role in the cancellation of RFI. ($\boldsymbol{v}$ is given directly for convenience, and this paper does not involve the measurement and estimation of $\boldsymbol{v}$).

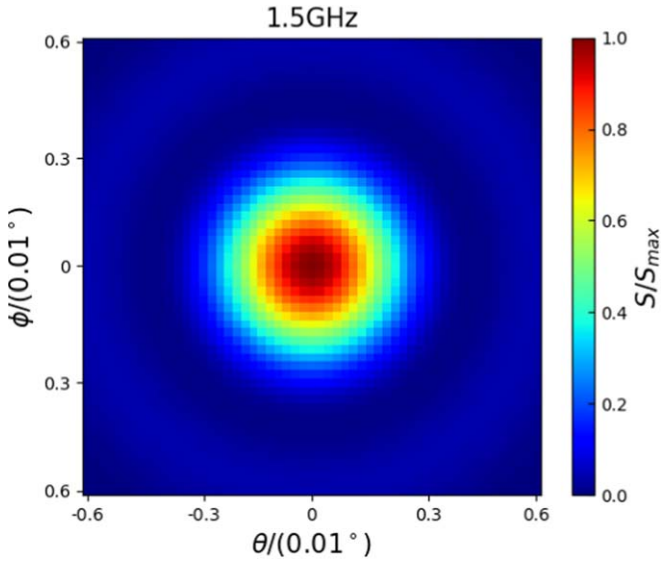

Figure 7. Normalized far-field pattern, resolution 55×55. The half-power beamwidth (HPBW) of QTT is 0°.025 at 1.5 GHz.

Visualization of Power: Radio astronomy often focuses on the measurement of celestial radiation power. In an STI of PAF, the average power can be measured by digital beam control. The expression is as follows:

$$\mathrm{P} = \omega R \omega \tag{9}$$

where ω is the normalized spatial direction vector. The power measurement in an STI can be realized by using this formula to traverse the imaging area.

3.2. The Influence of Coupling Matrix in PAF Beamforming

In order to analyze the influence of coupling coefficient in PAF beamforming, 32 of 96 QTT-PAF elements are selected to beamforming one beam. The distribution of these elements is shown in the selected ones in Figure 4, which are located in the center of the PAF and have good directional characteristic. The *Signal Generator* is used to generate an observation signal with a power far lower than that of noise and without RFI, which is to represent the scene when the telescope deep space exploration in a non-interference environment. The detailed parameters of the *Signal Generator* are shown in Table 1.

The *Signal Generator* generates two kinds of data, one with a coupling coefficient and the other without. As shown in Figure 8, the correlation matrices for these data are plotted separately, along with the correlation matrix for the coupling coefficient.

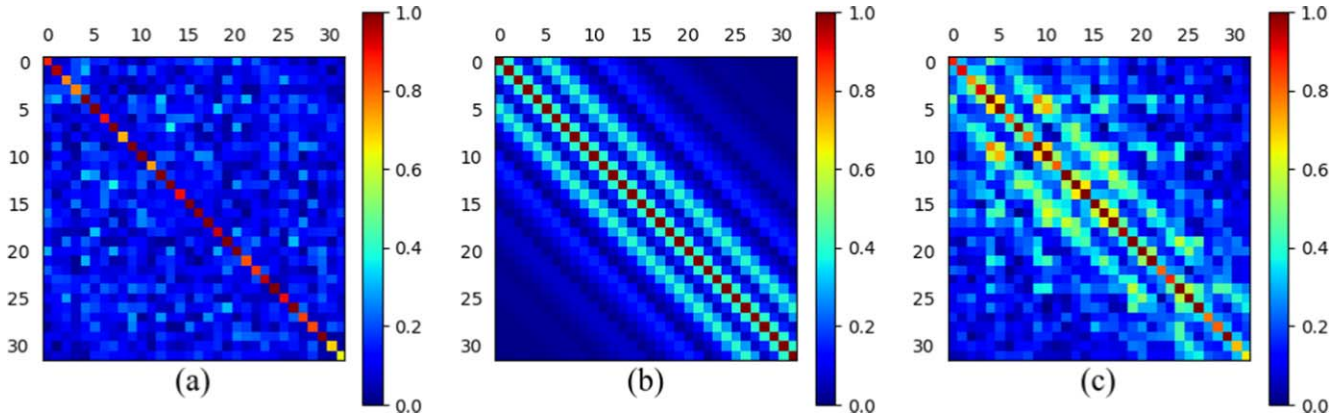

Figure 8. The correlation matrices of the two kinds of data generated by the *Signal Generator*, where STI = 4000. (a) Correlation matrix without a coupling coefficient in the data; (b) Correlation matrix when $\sigma = 0.4$; (c) Correlation matrix when the coupling coefficient is included in the data.

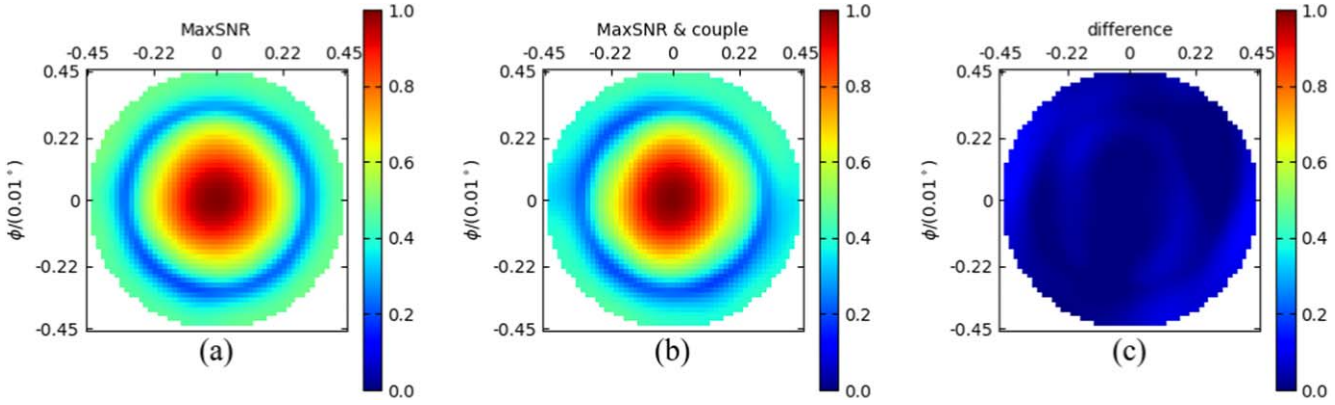

Figure 9. There are the 2D power images of the telescope in the data condition of Table 1. (a) shows the power image without the coupling matrix in the data. (b) The power image with coupling proof in the data set is displayed. (c) shows the power difference between the first two images.

Table 1
SOI Simulation Parameters

Parameters	SNR(in)/dB	SNR(out)/dB	$\theta/°$	$\phi/°$	f/GHz
SOI	−30	−30.99	0	0	1.5
RFI	null	null	null	null	null
noise		white noise			

From the correlation results in Figure 8, it can be seen that the coupling coefficient enhances correlation among elements while retaining the autocorrelation of conventional array. We use MaxSNR beamformer to complete beamforming of the results shown in Figure 8. In the ideal matching condition, the telescope pattern is obtained by weighting the *Main Reflector* and PAF pattern. We selected the area around the main lobe to draw 2D images using *Visualization of Power*, as shown in Figure 9.

It can be seen from Figure 9, when compared with data images without a coupling coefficient, the main lobe shape of the data images with a coupling coefficient is deformed, rotation symmetry is lost, and the first "null" depth is shallower. This is consistent with our understanding of the mutual coupling effects of PAF.

3.3. Subspace Projection Cancellation RFI

Subspace projection is an algorithm to control the "null" position of a telescope pattern. In the presence of interference, the SP algorithm uses projection operator P to cancel out RFI in the correlation matrix $\hat{\boldsymbol{R}}_x$ estimated by M × M dimension in an STI.

Normally in radio astronomy observation, the main lobe of a telescope is aligned with the target source, and the interference source enters through the sidelobe. The parameters in Table 2 are used to simulate the PAF array signal with coupling effect

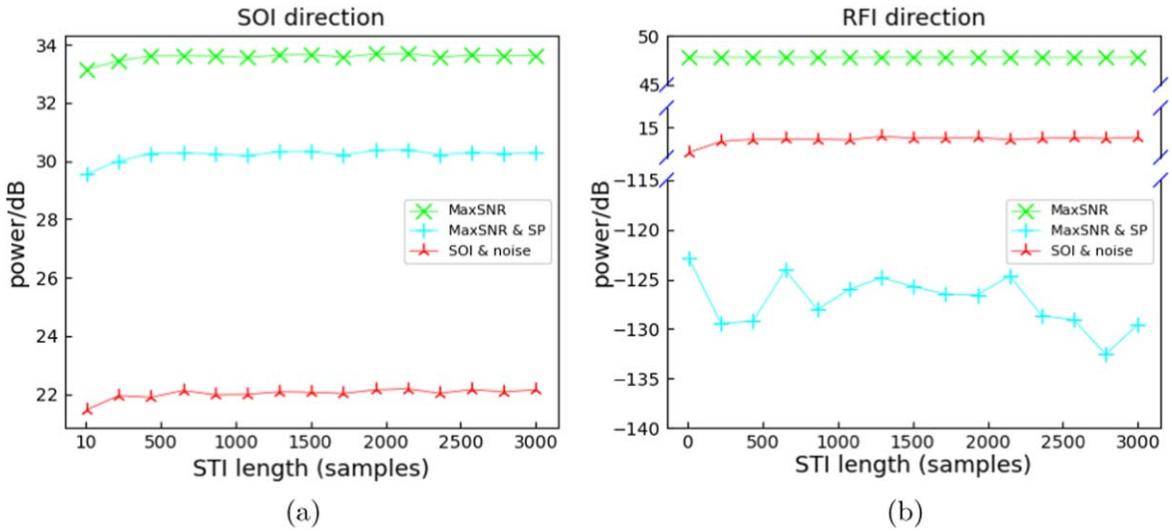

Figure 10. The SNR of the beamforming signals in the SOI and RFI directions. Here, the purple lines are the result of the MaxSNR beamformer; the red lines are the result of the *SP-Beamformer*; the cyan lines are the output of the MaxSNR beamformer with pure SOI (SOI and noise).

Table 2
SOI and RFI Simulation Parameters

Parameters	SNR(in)/dB	SNR(out)/dB	$\theta/^\circ$	$\phi/^\circ$	f/GHz
SOI	−30	−29.86	0	0	1.5
RFI	20	20.67	−0.6	0.6	1.5
noise		white noise			

by the *Signal Generator* when interference is present. It is assumed that there is only one interference source and its direction is random (excluding SOI direction).

We use the *SP-Beamformer* and MaxSNR beamformer to achieve beamforming against the elements signal, respectively. Then, the relationship between SNR and STI is calculated respectively in the direction of SOI and RFI, and the results are shown in Figure 10. In the results, we found that the presence of RFI in the beamforming has an effect on the power performance in the direction of SOI, and this effect is related to the size of STI. This is different from what we understood at the beginning.

In Figure 10(a), compared with the pure SOI results, the presence of RFI causes the energy to climb in the SOI direction. The main reason for this is the leakage of energy from the RFI direction to the SOI direction. After the beamforming of *SP-Beamformer*, the energy climb is improved, and this ability tends to a fixed value with the increase of STI size. In Figure 10(b), RFI is canceled by "null" after *SP-Beamformer* processing. The result of this deletion has a large dynamic range and will not be improved with the increase of STI size, but it can meet the requirement of RFI cancellation. In general, the SP algorithm can well meet the cancellation requirements of RFI, but it cannot fully restore the power of SOI, which is caused by $\boldsymbol{va} \neq 0$.

In conclusion, an appropriate increase of STI size can make the performance of the SP algorithm to restore SOI more stable, although the algorithm cannot be completely restored. For environments with strong RFI, the size of STI has less effect on cancellation because RFI dominates the signal power. Therefore, in the design of beamformer, the STI size should consider the stability of power restore in the direction of SOI while taking into account the performance of GPU.

Figure 11 is the sky power image of QTT, implemented by *Visualization of Power*. In Figure 11(a), the image after RFI failure can be shown that the RFI from the sidelobe is the main response area, while SOI response at the central position is covered up. Figure 11(b) is the image recovered by SP technology. It can be seen that RFI is completely eliminated and the response of SOI is highlighted. Figure 11(c) is the difference between the two figures.

4. Conclusion

The main content of this paper are as follows: (1) From the perspective of data correlation, the array data model which can reflect the coupling characteristic of planar PAF is established, and the coupling effect can lead to a loss of rotational symmetry and a shallower first "null". (2) The simulation of the combination of PAF and reflector antenna pattern is completed. The SP algorithm is used to cancel the RFI in PAF receiver and draw 2D power response images. Calculate the change of SOI power in RFI direction before and after using the SP algorithm.

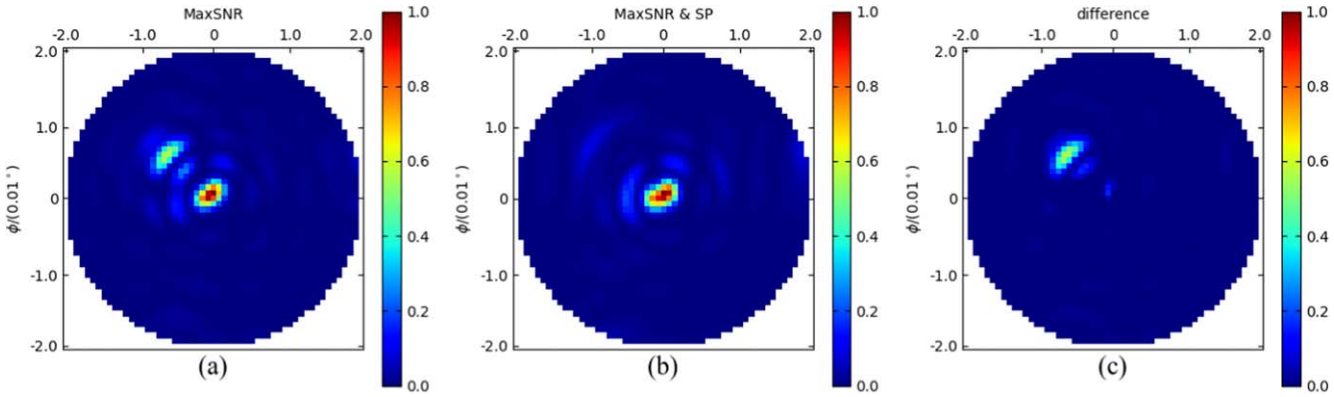

Figure 11. There is the 2D power image of QTT in the data condition of Table 2, STI = 2048.

Although the simulation of the model mentioned in the paper is mainly focused on the digital back end, without considering LNA, antenna efficiency, and other factors, the data model and simulation strategy can be used in the test to verify the beamformer and shorten the development time of the PAF receiver.

Acknowledgments

This work is funded by the National Key R&D Program of China under No. 2022YFC2205300, the National Natural Science Foundation of China (12073067), and the Chinese Academy of Sciences (CAS) "Light of West China" Program under No. 2022-XBQNXZ-012. P.W. would like to thank doctoral student Ya-Zhou Zhang of Xinjiang Astronomical Observatory for data processing.

References

Chai, X., Liu, B., & Zhu, Y. 2020, in 2020 XXXIIIrd General Assembly and Scientific Symposium of the International Union of Radio Science *(Rome, Italy)* (Piscataway, NJ: IEEE), 1
Chippendale, A. P., Beresford, R. J., Deng, X., et al. 2016, in 2016 International Conference on Electromagnetics in Advanced Applications (ICEAA) *(Cairns, Australia)* (Piscataway, NJ: IEEE), 909
Ivashina, M. V., Iupikov, O., Maaskant, R., et al. 2011, ITAP, 59, 1864
Landon, J., Jeffs, B. D., & Warnick, K. F. 2012, ITSP, 60, 1215
Li, J., Wu, P., Chen, M. J., et al. 2023, AcASn, 64, 1
Ma, J., Pei, X., Wang, N., et al. 2019, SSPMA, 49, 99502
Ma, J., Wu, Y., Xiao, S., et al. 2021, RAA, 21, 88
Nybo, J. M. 2019, "Development of a GPU-Based Real-Time Interference Mitigating Beamformer for Radio Astronomy" (2019), BYU Theses and Dissertations, 7749, https://scholarsarchive.byu.edu/etd/7749
Pei, X., Wang, N., Werthimer, D., et al. 2022, RAA, 22, 045016
Wang, K., Chen, M. J., Ma, J., et al. 2021, PABei, 39, 377
Wang, N. 2014, SSPMA, 44, 783
Warnick, K. F., Waldron, J., Landon, J., et al. 2007, in The Second European Conference on Antennas and Propagation, EuCAP 2007 (Edinburgh: IET), 1